Fluorescent Nanoparticles

International Edition: DOI: 10.1002/anie.201506171
German Edition: DOI: 10.1002/ange.201506171

Organized Aggregation of Porphyrins in Lipid Bilayers for Third Harmonic Generation Microscopy

*Liyang Cui, Danielle Tokarz, Richard Cisek, Kenneth K. Ng, Fan Wang, Juan Chen, Virginijus Barzda, and Gang Zheng**

Abstract: *Nonlinear optical microscopy has become a powerful tool for high-resolution imaging of cellular and subcellular composition, morphology, and interactions because of its high spatial resolution, deep penetration, and low photo-damage to tissue. Developing specific harmonic probes is essential for exploiting nonlinear microscopic imaging for biomedical applications. We report an organized aggregate of porphyrins (OAP) that formed within lipidic nanoparticles showing fingerprint spectroscopic properties, structure-associated second harmonic generation, and superradiant third harmonic generation. The OAP facilitated harmonic microscopic imaging of living cells with significantly enhanced contrast. The structure-dependent switch between harmonic (OAP-intact) and fluorescence (OAP-disrupted) generation enabled real-time multi-modality imaging of the cellular fate of nanoparticles. Robustly produced under various conditions and easily incorporated into pre-formed lipid nanovesicles, OAP provides a biocompatible nanoplatform for harmonic imaging.*

Nonlinear optical microscopy (NLOM) has invigorated many research fields over the past decades, expanding its application from molecular interactions to intravital imaging.[1] NLOM of third harmonic generation (THG)[2] enables observation of the interface of two materials with different refractive indexes, such as the interface between an aqueous medium and a lipidic or absorbing structure, to provide convenient mapping of innate heterogeneities in biological samples.[3] However, label-free THG imaging generally lacks selectivity to the target of interest.[4] Therefore, exogenous harmonic generation tracers, termed harmonophores, are involved to enhance the imaging contrast and labeling specificity. Inorganic harmonophores are far more mature than organic ones. Examples of inorganic harmonophores include $LiNbO_3$ crystals,[5] quantum dots,[6] gold nanoparticles,[7] and indium tin oxide nanoparticles,[8] but their biomedical implementation was hindered by concerns on lack of biocompatibility and biosafety. Herein, we introduce an all-organic system containing an organized aggregate of porphyrins (OAP) built within lipid layers of nanoparticles, which showed structure-driven spectroscopic properties and strong harmonic generation. OAP was not only a superradiant harmonophore, but exhibited a modality switch from harmonic generation to fluorescence between intact and disrupted OAP. The biocompatible nature of porphyrin materials of OAP made it an ideal bio-friendly harmonophore with built-in optical components to monitor the fate of the host nanovehicles.

The OAP formed spontaneously when rehydrating a lipid film containing a porphyrin molecule, pyropheophorbide *a* (pyro). Transmission electron microscopy (TEM) and dynamic light scattering revealed a spherical liposome-like structure of the resulting particles sized around 100 nm (Figure 1 a; Supporting Information, Figure S1). A thickened lipid bilayer (23.8 ± 3.9 nm vs ~4.0 nm for liposomes)[9] was observed at high magnification of TEM, likely owing to the pyro embedment and aggregation. The presence of ordered pyro aggregation in the particle was determined spectroscopically by the narrow absorption band red-shifted with respect to pyro monomer band and huge Cotton split in the circular

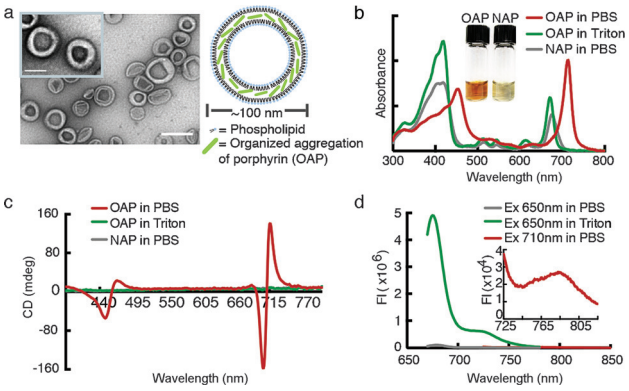

Figure 1. Formation and characterization of organized aggregate of porphyrin in lipid layers. a) Transmission electronic micrographs of lipidic nanoparticle containing OAP (scale bar: 200 nm, inset scale: 100 nm) with illustration of OAP residing in between lipid layers. b) UV/Vis spectra of intact (in PBS) and disrupted (by detergent) OAP- and NAP-nanoparticles. Inset image shows freshly prepared OAP- and NAP-particle solutions. c) Circular dichroism spectra of OAP- and NAP-nanoparticles. d) Fluorescence emission spectra of intact and disrupted OAP-nanoparticle excited at the Qy absorption band.

[*] Dr. L. Cui, Dr. K. K. Ng, Dr. J. Chen, Prof. G. Zheng
Princess Margaret Cancer Center and Techna Institute, UHN (Canada)
E-mail: gang.zheng@uhnres.utoronto.ca
Homepage: http://www.utoronto.ca/zhenglab
Dr. L. Cui, Prof. F. Wang
Medical Isotopes Research Center
Peking University (China)
Dr. L. Cui, Prof. G. Zheng
Department of Medical Biophysics
University of Toronto (Canada)
Dr. D. Tokarz, Dr. R. Cisek, Prof. V. Barzda
Department of Chemical and Physical Sciences and
Department of Physics, University of Toronto (Canada)

Supporting information for this article is available on the WWW under http://dx.doi.org/10.1002/anie.201506171.

dichroism (CD) spectrum. The pronounced increase in the Q_y absorption band red-shifted from 671 nm to 712 nm was ascribed to the extended π interactive system (Figure 1b). The bisignate psi-type CD signals indicated strong excitonic couplings of the electric dipole transition moment between pyro molecules in the supermolecular structure[10] (Figure 1c). When added with detergent, the OAP dissociated and lost its chirality.[11] Notably when pyro was conjugated to an alkyl side chain of the lipid, such as in the case of previously reported porphyrin-nanovesicle porphysomes,[12] it behaved rather like amphiphilic lipids and was involved in the lipid bilayer formation with homogeneous distribution, thus resulted in a limited π-π interaction (3 nm Q_y band shift). Consistently, no split band was observed in the CD spectrum of pyro-lipid nanoparticles. We herein call this type of segregated porphyrin in lipid layers (without forming organized aggregate) as non-organized aggregate of porphyrin (NAP), which served as a control to extensively study the photoproperties of OAP. Corresponding to the red-shift absorption, OAP emitted completely red-shifted fluorescence peaking at 785 nm with extremely low intensity (Figure 1d). The highly quenched fluorescence can be relieved by the disruption of OAP with detergent, where the fluorescence of monomeric pyro at 675 nm was promptly restored with 200-fold intensity increase (Figure 1d). These results indicated the unique structure-associated spectroscopic properties of OAP.

The OAP could be formed easily in a lipid environment, but not in other solvent condition (Supporting Information, Figure S2). The formed, OAP is stable in storage over 30 days, exhibiting no significant change in the particle size (104.0 ± 20.8 nm) and absorption/CD spectrum properties (Supporting Information, Figure S3). However, enzymatic decomposition of the lipid layer led to immediate disassembly of the OAP structure (Supporting Information, Figure S4), verifying the importance of the lipid scaffold for stabilizing OAP. With the support of the lipid scaffold, OAP can be robustly produced under various conditions, including different lipid constituents, pH, cholesterol content, pyro/lipid molar ratios, and surface charge of the particles. OAP was found to form in rehydrating solutions with a wide range of pH (4.5-10.5) with no noticeable changes at the Q_y absorption (Figure 2a). Similarly, cholesterol content had no effect on the formation of OAP (Figure 2b). The assembly of pyro into OAP was not affected by the hydrocarbon chain length of the phospholipid, but may be affected by the unsaturation of the host lipid as a result of its low transition temperature (T_m). For example, dual Q_y band absorption peaks were observed when pyro assembled in POPC ($T_m = -2\,°C$) nanoparticles (Figure 2c), suggesting the coexistence of the organized and non-organized pyro assembly, which might result from the partial destruction of OAP caused by the disorder of the host lipid layer in liquid crystalline phase at room temperature.

The lipid scaffold could also modulate OAP formation through electrostatic forces. When host lipids were positively charged (ζ potential of 4.5 ± 1.9 mV), pyro molecules tend to assemble in a non-organized pattern (Figure 2d). With the increase of negative charge of particles, a gradual increase in the OAP Q_y absorption band (Figure 2d) and amplitude of

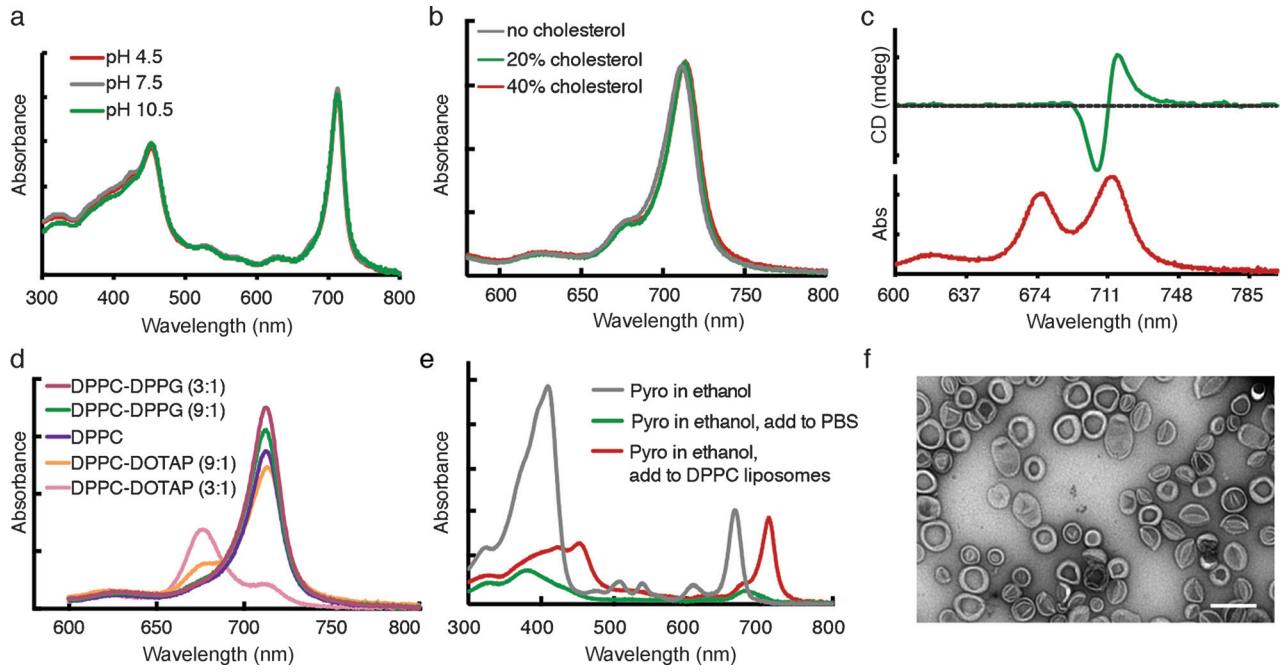

Figure 2. Robust formation of OAP under various host environments. a) UV/Vis spectra of OAP-nanoparticles formulated with solutions of pH 4.5, 7.5 and 10.5. b) UV/Vis of OAP in nanoparticles consisting of DPPC and 0%, 20% and 40% (mol%) cholesterol. c) UV/Vis and CD spectra of OAP in nanoparticles composed of unsaturated lipid POPC. d) Surface charge effect of the host particles on the formation of OAP. The surface charge of lipid layer was modulated by incorporating different molar percentages of positively charged lipid, DOTAP, or negatively charged lipid, DPPG. Fingerprint OAP Qy absorption band of each formulation was evaluated. e) UV/Vis spectra of pyro before and after addition to DPPC liposomes, showing the post-insertion capability of OAP into the pre-formed liposomes. Pyro solution added to PBS buffer was used as control. f) TEM image of DPPC liposomes post-inserted with OAP (scale: 200 nm).

the split in CD were observed (Supporting Information, Figure S5c,d), suggesting that the electrostatic repulsion between the lipid and pyro facilitated the confinement and re-orientation of pyro molecules. This result demonstrated that OAP could be micro-adjusted by tuning the charge of lipid layers.

Intriguingly, when mixed with pre-formed liposome solutions, pyro monomers incorporated into the particles and formed OAP promptly (Q_y band red-shift from 666 nm to 712 nm, Figure 2e). The particles with post-inserted OAP exhibited similar size and morphology in TEM compared to those formulated with films of mixture (Figure 2f) and were functionally stable (Supporting Information, Figure S6). This post-insertion approach provides a robust way to produce OAP in pre-formed lipidic vesicles, thus leading OAP to a broad array of future applications.

We started characterizing the nonlinear optical properties of OAP by imaging with second harmonic generation (SHG) and THG microscopy. A significant increase of SHG signal (4.7-fold increase) was observed in OAP samples when compared to NAP samples where porphyrins are segregated through nanoparticles without forming OAP aggregate (Figure 3a), indicating a crystalline structure of OAP where the pyro molecules were arranged noncentrosymmetrically in agreement with CD observations. Since porphyrin molecules are known to have large third-order nonlinear optical properties,[13] THG signal is expected for both OAP and NAP. However, OAP showed a significantly stronger THG signal (5.3-fold increase) than NAP at the same pyro concentration (Figure 3b), suggesting that THG is remarkably enhanced by the supermolecular structure of OAP. THG requires the instantaneous capture of three photons by the materials to create a new photon having three times the energy (Figure 3b), therefore a cubic dependence of the radiated THG with excitation intensity was expected. An exponential increase in the emitted signal with a power of 2.8 ± 0.2 on the excitation intensity was observed (Supporting Information, Figure S7), confirming that the signal collected from OAP was attributed to the third-order optical nonlinearity.

An important aspect for dye aggregates that show nonlinearity is the size-enhancement, where the hyperpolarizabilities scale not proportionally, but rather in a N^{α} fashion ($\alpha \geq 2$) to the number of molecules (N) it contains.[14] This superradiance effect resulting from the intermolecular interactions offers the aggregates a superior state relative to incremental increases in dye concentration. By formulating samples with varied molar ratios of pyro/lipid, a series of OAP with different aggregation scales were achieved. The growth of OAP was seen by a gradual increase in the absorption bands and CD amplitude until reaching the maximum loading of the pyro (~20 mol%; Figure 3c-d; Supporting Information, Figure S8). Excitingly, an exponential increase in the THG intensity with a power of 2.33 ± 0.53 was observed with increasing pyro molar ratio (Figure 3e). This slightly higher observed power (2 for THG theoretically) is likely attributed to excitonic interactions that occur within the aggregate, leading to exciton-superradiance.[15]

Photobleaching is one major concern for fluorescent dyes. In comparison, harmonophores which do not absorb light at the fundamental laser or harmonic wavelengths are excited to their higher energy state with a virtual energy transition, which does not require any internal relaxation and energy loss. The 1/*e* lifetime of OAP was 8.4 min at pulse energy of 1 nJ (13.9 mW) and found up to 42.7 min at 0.4 nJ pulse energy (5.9 mW) with no significant decrement in the THG signal (Figure 3f). At a higher pulse energy of 2 nJ (29.4 mW), OAP photobleached with a 1/*e* lifetime of 2.4 min, owing to the pyro absorption at the third harmonic wavelength of the laser (343 nm). This suggests that OAP is highly photostable as a harmonophore and is able to generate THG signals with minimal fluctuation under continuous irradiation at lower power range.

Having demonstrated the versatility and high harmonic generation, we sought to apply this radiant harmonophore for cell labeling and imaging. A gradual enhancement of the THG signals was observed in PC-3 living cells with increase of incubation time (Figure 4a), indicating a time-dependent uptake process of OAP-nanoparticles. After 40 min incuba-

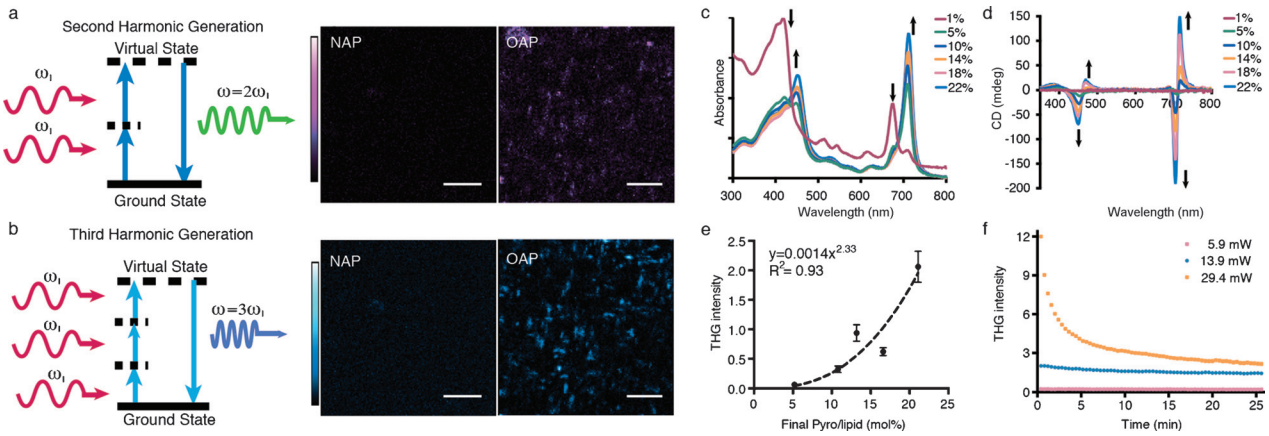

Figure 3. Structure-dependent high harmonic generation of OAP. a) Energy-level diagram (left) describing second harmonic generation (SHG) with SHG images of NAP and OAP immobilized in polyacrylamide gel (right, scale: 10 μm). b) Energy-level diagram (left) describing third harmonic generation (THG) with THG images of NAP and OAP (right, scale: 10 μm). c) UV/Vis spectra of OAP with different pyro molar percentages to lipid. d) CD spectra of OAP with different pyro molar percentages to lipid. e) THG intensity as a function of molar percentage of pyro, showing a power dependence of 2.33. f) Photobleaching of OAP under continuous laser irradiation at different laser intensities.

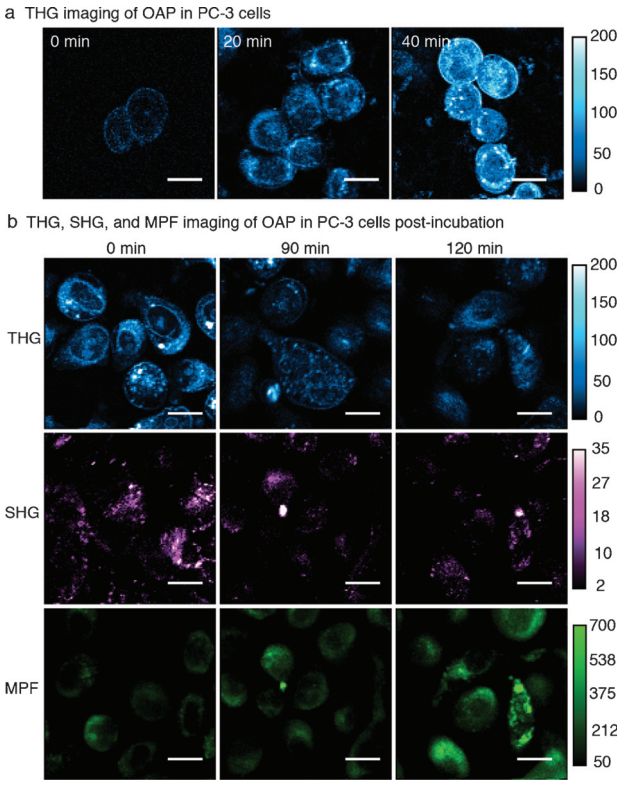

Figure 4. Multi-channel nonlinear imaging of cells incubated with OAP-nanoparticles. a) THG imaging of the PC-3 cell suspension at pre-incubation and 20 min and 40 min after incubation (scale: 20 μm). b) PC-3 cells were incubated with OAP particles for 40 min and subsequently imaged at 0, 90, and 120 min post-incubation with THG, SHG, and MPF (scale: 20 μm). The three signals were acquired simultaneously at each time point and normalized to the same settings respectively for each modality.

tion, cells were clearly delineated with significantly contrast-enhanced THG. More importantly, the distinct optical properties of the intact (harmonic generation) and the disrupted form (multiphoton fluorescence, MPF) of OAP made it an excellent self-reporter to track the metabolic dynamics upon uptake by the cells. SHG and THG signals were the strongest whereas MPF was the weakest right after 40 min incubation when most OAP remained intact and quenched in the cells (Figure 4b). As the host nanoparticles were being metabolized and degraded, OAP started to disassemble, leading to a decrease in the structure-driven SHG and THG signals and an increase in the fluorescence emitted by pyro monomers. After 120 min, most OAP was disrupted and fluorescence increased while SHG and THG signals dramatically decreased. As a nonlinear-optically switchable label, OAP enabled a real-time three-channel feedback of its integrity, thus providing complementary information on the fate of the host-particles.

Natural and biomimetic chlorophyll aggregates have been extensively investigated for optoelectronics, photosynthesis, and photosensitization[16] owing to their favorable structure-associated spectroscopic and optical properties, but studies on their nonlinear optical properties are limited.[17] In our study, different pyro assembly patterns showed distinct optical properties and the formation of microcrystalline OAP rendered high SHG and THG. OAP can be easily carried and delivered within lipidic nanoconstructs, and are able to enhance the THG signal remarkably once accumulated in cells. The structure-driven nonlinear optical properties of OAP cause a transformation-induced imaging modality shift; that is, once the assembly is disrupted, it will shift from SHG and THG to fluorescent signals. By imaging MPF, SHG, and THG signals with a multimodal microscope, we could visualize the uptake, degradation, and clearing-out of the nanoparticles. Therefore, OAP can be used not only as a radiant harmonophore, but also as multifunctional imaging and therapeutic component that provides real-time information regarding the state of the supporting nanoparticles for accurate dosimetry.

Deciphering the structure of chlorophyll aggregates is quite challenging owing to the structural variety and the absence of single-crystal X-ray data. In our study, the unique spectroscopic and optical properties of OAP provided insights into the arrangement of the porphyrin molecules. A pronounced bathochromic shift in the porphyrin Qy absorption band from 671 nm (monomeric) to 712 nm (assembled), and Soret band from 418 nm to 452 nm were revealed in the absorption spectra, indicating an extended π interactive system in between porphyrins. The [−/+] bisignate curve from shorter to longer wavelength in the CD spectrum in OAP particles indicated a clock-wise arrangement of porphyrin in the chiral array. The intrinsic polarization-dependent harmonic generation property of OAP may offer more information to elucidate the organization of pyro molecules in the aggregates. Using the polarization-resolved second harmonic generation technique, the second-order nonlinear optical susceptibility component ratio, $\chi^{(2)}_{ZZZ'}/\chi^{(2)}_{ZXX'}$, for this OAP was found to be 2.5 ± 0.2 (Supporting Information, Figure S9). Further understanding could be achieved by modelling absorption and susceptibility of the nanoparticles with ab initio calculations. Initio calculations and fitting the models to the susceptibility matches the results observed experimentally.

In summary, confining naturally derived porphyrins in an organized aggregation state within lipid bilayers, OAP is a highly biocompatible and biodegradable component that can be easily fabricated into lipid-based particles. The aggregates are versatile, and the structure-driven switch of OAP among imaging modalities extends the contrast mechanism of high harmonic generation microscopy from innate signal changes to the direct responsiveness of exogenous agents.

Acknowledgements

The authors thank Dr. Brian Wilson for insightful discussion and funding support from the Natural Sciences and Engineering Research Council of Canada, Canadian Institutes of Health Research, Terry Fox Research Institute, Major International (Regional) Joint Research Project from National Science foundation of China, Canada Foundation for Innovation, and the Joey and Toby Tanenbaum/Brazilian

Ball Chair in Prostate Cancer Research and the Princess Margaret Cancer Foundation.

Keywords: harmonic generation · multimodality imaging · nonlinear optical properties · organized aggregation · porphyrin nanoparticles

How to cite: *Angew. Chem. Int. Ed.* **2015**, *54*, 13928–13932
Angew. Chem. **2015**, *127*, 14134–14138

[1] a) B. J. Bacskai, S. T. Kajdasz, R. H. Christie, C. Carter, D. Games, P. Seubert, D. Schenk, B. T. Hyman, *Nat. Med.* **2001**, *7*, 369–372; b) D. R. Larson, W. R. Zipfel, R. M. Williams, S. W. Clark, M. P. Bruchez, F. W. Wise, W. W. Webb, *Science* **2003**, *300*, 1434–1436; c) N. Olivier, M. A. Luengo-Oroz, L. Duloquin, E. Faure, T. Savy, I. Veilleux, X. Solinas, D. Debarre, P. Bourgine, A. Santos, N. Peyrieras, E. Beaurepaire, *Science* **2010**, *329*, 967–971; d) K. Svoboda, D. W. Tank, W. Denk, *Science* **1996**, *272*, 716–719; e) E. B. Voura, J. K. Jaiswal, H. Mattoussi, S. M. Simon, *Nat. Med.* **2004**, *10*, 993–998; f) J. H. Yu, S. H. Kwon, Z. Petrasek, O. K. Park, S. W. Jun, K. Shin, M. Choi, Y. I. Park, K. Park, H. B. Na, N. Lee, D. W. Lee, J. H. Kim, P. Schwille, T. Hyeon, *Nat. Mater.* **2013**, *12*, 359–366.

[2] Y. Barad, H. Eisenberg, M. Horowitz, Y. Silberberg, *Appl. Phys. Lett.* **1997**, *70*, 922–924.

[3] a) V. Barzda, C. Greenhalgh, J. Aus der Au, S. Elmore, J. van Beek, J. Squier, *Opt. Express* **2005**, *13*, 8263–8276; b) D. Débarre, W. Supatto, A. M. Pena, A. Fabre, T. Tordjmann, L. Combettes, M. C. Schanne-Klein, E. Beaurepaire, *Nat. Methods* **2006**, *3*, 47–53; c) M. Muller, J. Squier, K. R. Wilson, G. J. Brakenhoff, *J. Microsc.* **1998**, *191*, 266–274; d) C. K. Sun, *Adv. Biochem. Eng. Biotechnol.* **2005**, *95*, 17–56.

[4] S. Witte, A. Negrean, J. C. Lodder, C. P. de Kock, G. T. Silva, H. D. Mansvelder, M. L. Groot, *Proc. Natl. Acad. Sci. USA* **2011**, *108*, 5970–5975.

[5] S. Kiyotaka, T. Masahiro, *Appl. Phys. Express* **2009**, *2*, 122401.

[6] C. F. Chang, C. Y. Chen, F. H. Chang, S. P. Tai, C. Y. Chen, C. H. Yu, Y. B. Tseng, T. H. Tsai, I. S. Liu, W. F. Su, C. K. Sun, *Opt. Express* **2008**, *16*, 9534–9548.

[7] a) M. Lippitz, M. A. van Dijk, M. Orrit, *Nano Lett.* **2005**, *5*, 799–802; b) O. Schwartz, D. Oron, *Nano Lett.* **2009**, *9*, 4093–4097.

[8] H. Aouani, M. Rahmani, M. Navarro-Cia, S. A. Maier, *Nat. Nanotechnol.* **2014**, *9*, 290–294.

[9] P. Balgavý, M. Dubnicková, N. Kucerka, M. A. Kiselev, S. P. Yaradaikin, D. Uhriková, *Biochim. Biophys. Acta Biomembr.* **2001**, *1512*, 40–52.

[10] a) V. Barzda, L. Mustardy, G. Garab, *Biochemistry* **1994**, *33*, 10837–10841; b) "Exciton Coupling and Exciton Chirality": D. A. Lightner, J. E. Gurst in *Organic Conformational Analysis and Stereochemistry from Circular Dichroism*, Wiley-VCH, New York, **2000**, pp. 423-454.

[11] J. M. Ribo, J. Crusats, F. Sagues, J. Claret, R. Rubires, *Science* **2001**, *292*, 2063–2066.

[12] J. F. Lovell, C. S. Jin, E. Huynh, H. Jin, C. Kim, J. L. Rubinstein, W. C. Chan, W. Cao, L. V. Wang, G. Zheng, *Nat. Mater.* **2011**, *10*, 324–332.

[13] a) D. Tokarz, R. Cisek, N. Prent, U. Fekl, V. Barzda, *Anal. Chim. Acta* **2012**, *755*, 86–92; b) M. O. Senge, M. Fazekas, E. G. A. Notaras, W. J. Blau, M. Zawadzka, O. B. Locos, E. M. Ni Mhuircheartaigh, *Adv. Mater.* **2007**, *19*, 2737–2774.

[14] E. Hanamura, *Phys. Rev. B* **1988**, *37*, 1273–1279.

[15] J. Knoester, *Chem. Phys. Lett.* **1993**, *203*, 371–377.

[16] M. K. Panda, K. Ladomenou, A. G. Coutsolelos, *Coord. Chem. Rev.* **2012**, *256*, 2601–2627.

[17] a) R. Cisek, L. Spencer, N. Prent, D. Zigmantas, G. S. Espie, V. Barzda, *Photosynth. Res.* **2009**, *102*, 111–141; b) D. Tokarz, R. Cisek, U. Fekl, V. Barzda, *J. Phys. Chem. B* **2013**, *117*, 11069–11075; c) "Non-Linear Contrast Mechanisms for Optical Microscopy": V. Barzda in *Biophysical Techniques in Photosynthesis, Vol. 26* (Eds.: T. Aartsma, J. Matysik), Springer Netherlands, **2008**, pp. 35–54.

Received: July 5, 2015
Revised: August 28, 2015
Published online: September 29, 2015

